Residential Battery Modeling for Control-Oriented Techno-Economic Studies

Preprint

Rohit Chintala, Ben Polly, Xin Jin, Dane Christensen, and Noel Merket

National Renewable Energy Laboratory

Presented at the 2020 ACEEE Summer Study on Energy Efficiency in Buildings
August 17–21, 2020

NREL is a national laboratory of the U.S. Department of Energy
Office of Energy Efficiency & Renewable Energy
Operated by the Alliance for Sustainable Energy, LLC

This report is available at no cost from the National Renewable Energy Laboratory (NREL) at www.nrel.gov/publications.

Contract No. DE-AC36-08GO28308

Conference Paper
NREL/CP-5500-76065
September 2020

Residential Battery Modeling for Control-Oriented Techno-Economic Studies

Preprint

Rohit Chintala, Ben Polly, Xin Jin, Dane Christensen, and Noel Merket

National Renewable Energy Laboratory

Suggested Citation
Chintala, Rohit, Ben Polly, Xin Jin, Dane Christensen, and Noel Merket. 2020. *Residential Battery Modeling for Control-Oriented Techno-Economic Studies: Preprint*. Golden, CO: National Renewable Energy Laboratory. NREL/CP-5500-76065.
https://www.nrel.gov/docs/fy20osti/76065.pdf.

NREL is a national laboratory of the U.S. Department of Energy
Office of Energy Efficiency & Renewable Energy
Operated by the Alliance for Sustainable Energy, LLC

This report is available at no cost from the National Renewable Energy Laboratory (NREL) at www.nrel.gov/publications.

Contract No. DE-AC36-08GO28308

Conference Paper
NREL/CP-5500-76065
September 2020

National Renewable Energy Laboratory
15013 Denver West Parkway
Golden, CO 80401
303-275-3000 • www.nrel.gov

NOTICE

This work was authored by the National Renewable Energy Laboratory, operated by Alliance for Sustainable Energy, LLC, for the U.S. Department of Energy (DOE) under Contract No. DE-AC36-08GO28308. Funding provided by U.S. Department of Energy Office of Energy Efficiency and Renewable Energy Building Technologies Office. The views expressed herein do not necessarily represent the views of the DOE or the U.S. Government.

Cover Photos by Dennis Schroeder: (clockwise, left to right) NREL 51934, NREL 45897, NREL 42160, NREL 45891, NREL 48097, NREL 46526.

Residential Battery Modeling for Control-Oriented Techno-Economic Studies

Rohit Chintala, Ben Polly, Xin Jin, Dane Christensen, Noel Merket
National Renewable Energy Laboratory

ABSTRACT

Electrochemical batteries, which serve as electric energy storage devices, are becoming increasingly popular among residential buildings that incorporate solar photovoltaic (PV) systems to help meet their energy needs. Battery economics are affected by performance degradation over time, and managing this degradation can help extend the battery's lifespan. The tradeoff between operational costs/benefits and managing battery degradation is of significant research interest. One of the key factors for assessing battery degradation is the dispatch strategy used to control the charging and discharging of the battery. Conventional dispatch strategies typically use simple rule-based methods, and these overly aggressive charging/discharging cycles can significantly reduce a battery's life span. Our research seeks to develop optimized dispatch strategies for grid-connected PV homes with a goal of extending battery life while simultaneously taking into consideration utility costs and occupant comfort. To achieve this goal, we adapted lithium-ion battery life- and cyclic-degradation models for use in high-fidelity building simulations, so whole-building and grid-interactive controllers can dispatch the batteries along with other flexible loads. With the help of a co-simulation platform, we performed a simulation study to compute the optimized dispatch strategies for relevant operating conditions brought about by changing geographical locations, weather conditions, and utility pricing. Comparing the optimized strategies with the conventional strategies resulted in a >50% decrease in capacity degradation and >10% average reduction in operational costs during the months of January and July in Fort Collins, Colorado; Phoenix, Arizona; and Portland, Oregon.

Introduction

Homeowners in the United States are increasingly adopting distributed power generation through on-site solar photovoltaic (PV) systems. Over 2 million residential homes in the United States had PV systems installed by the end of 2018, constituting 1.7% of households, and the total number is expected to exceed 3 million by 2021 (Feldman 2019) The operating hours when energy is produced by PV systems, however, do not typically coincide with residential demand peaks. Thus, storage devices such as electric batteries can substantially increase the utilization of PV systems because they help in balancing energy production with demand (Toledo 2010). Batteries can provide other significant benefits to homes, such as increasing reliability and sustainability of available power, reducing dependence on the electric grid, and lowering utility bills under certain rate structures (Toledo, 2010; Mishra 2020). These potential benefits of employing home battery systems coupled with tax incentives, declining costs of batteries, and a greater penetration of time-of-use (TOU) utility pricing has led to increasing adoption of behind-the-meter residential battery energy systems (BES). For example, just by the end of Q3 of 2019, the United States witnessed a 40-MWh increase over 2018 in deployment of residential BES (Feldman 2019).

The cost-effectiveness of a BES is highly dependent on the particular operational savings that can be achieved relative to the price of the BES. The price of BES is determined by several technical characteristics, such as its total power and energy capacity (U.S. EIA 2018). In 2019, the U.S. market prices of battery systems for small residential applications were around $171 per kWh and $970 per kW, with the installation adding a fixed cost of around $400 (Comello 2019). One study found that, on average, a small residential home with a grid-connected PV system requires about a 3-kWh battery to support a critical load, which is generally 15% of its average daily energy consumption (Hoff 2004). Thus, a 3-kWh residential BES with 3-kW power providing critical load support would cost around $4,000. The cost-effectiveness of residential BES is also affected by the degradation in the total charge capacity over time, which can impact the operational (utility bill) cost savings and total lifetime of the BES. The degradation of battery capacity, also referred to as battery aging, is significantly impacted by the charging and discharging strategies used to store and release electric energy, respectively. The charging and discharging strategies (dispatch strategies) are governed by a control technology that regulates key features of the battery packs such as state of charge (SOC) and depth of discharge (DOD). The control technology also provides the opportunity for users to increase the value of residential BES by increasing PV self-consumption and providing grid services such as load shifting, demand reduction, and frequency regulation (Fitzgerald 2015). Advancements in battery manufacturing technology can thus be complemented with improvements in control technology to enhance the cost-effectiveness of energy storage. The co-simulation platform proposed in this research would serve as a valuable tool in determining and validating the new control technologies.

This paper first presents a high-fidelity simulation platform for studying different control technologies, taking into consideration both battery aging and occupant comfort. Using a typical large single-family home as a test case, the paper then develops optimized dispatch strategies for the grid-connected PV home with a goal of extending battery life while simultaneously reducing utility costs and maintaining occupant comfort. We compute optimal dispatch strategies for different operating conditions brought about by changing weather conditions, comfort thresholds, and utility rate structures.

Several past research efforts have extensively studied energy management strategies for homes and commercial buildings with grid-connected PV and batteries (Gitizadeh 2013; Pascual 2015; Nottrott 2013; Riffonneau 2011; Li 2014). For example, the authors in (Gitizadeh 2013) proposed a sizing and dispatch-scheduling strategy under TOU and demand-charge pricing using mixed-integer programming to solve an optimization problem that minimized utility pricing and battery degradation. Similarly, the authors in (Nottrott 2013) proposed a method to compute optimized dispatch schedules for grid-connected PV-battery systems using a linear programming routine. For this study, we performed the optimization every 15 minutes and relied on forecasts of PV power and building loads over a forward-looking 24-hour time horizon. These earlier studies developed strategies using simple constant-power models and a simplified battery-degradation model. Furthermore, the studies considered building loads as an uncontrollable input and thus did not include building load flexibility in the formulation of their objective function. Research efforts to find optimized battery control strategies for commercial buildings using a much higher fidelity battery-degradation model were conducted by the authors in (Cai 2019). The authors compared the impacts of model predictive control (MPC) strategies and two rule-based strategies on utility costs and battery degradation under TOU and demand-charge rate structures.

The work presented in this paper builds on the aforementioned research on optimized control methods for grid-connected PV battery systems for residential buildings in the following ways:

- Developing a platform that utilizes high-fidelity models of both the building thermodynamics and battery degradation
- Considering the effects of ambient temperature on usable capacity and capacity degradation in the computation of the optimized control strategies
- Summarizing the impacts of the proposed optimized control strategies under different operating conditions brought about by changing weather conditions, utility rate structures, and comfort constraints for a typical large single-family home.

This work is part of a broader effort to enhance residential building energy modeling capabilities to support the analysis of grid-interactive efficient buildings (GEBs). GEBs can provide benefits to homeowners and the grid through a combination of efficiency and demand flexibility strategies (Neukomm 2019). Having accurate models of behind-the-meter residential stationary batteries and their controls is critical to understanding the potential synergies and tradeoffs that batteries have with other building demand flexibility strategies and ultimately for developing optimized solutions from a whole-home integration perspective.

Simulation and Control Platform

A simulation platform is useful to develop and optimize dispatch strategies for homes with PV and batteries before they are implemented in the real world. The accuracy of the simulation environment has a substantial impact when computing these strategies, such as in quantifying the energy and cost savings that varying operating conditions can achieve. One of the unique contributions of this research is using the high-fidelity building energy simulation engine in EnergyPlus™ (U.S. Department of Energy's [DOE's] whole-building energy simulation program) and an experimentally validated lifetime charge degradation model developed by Smith et al. in (Smith 2017) as a simulation test bed. When combined, these simulation models allow us to explore the impacts of different operating conditions and control strategies on the battery life span, utility costs, and energy consumption of the home.

We developed the proposed optimized control strategy using MPC, which minimizes an objective function to compute the control actions. Reduced-order models of the simulation system are required to make the optimization problem computationally feasible. MPC relies on predictions from the reduced-order models to compute the optimal trajectory that minimizes the objective function over a prediction horizon. We developed the co-simulation platform is developed by leveraging previous work completed by Jin et.al in (Jin 2017), augmented with a linear parametric autoregressive with extra input (ARX) model for building thermodynamics, battery electric performance, and degradation models (both simulation and reduced-order). The reduced-order model of the building thermodynamics and the battery degradation model are novel contributions of this research.

The co-simulation platform thus comprises simulation and reduced-order models of the building thermodynamics, water heater, and battery, as shown in Figure 1. The control actions computed by the MPC are duty cycles U_{hvac}, U_{wh}, and U_{bat}, which regulate the heating, ventilating, and air-conditioning (HVAC) system, water heater, and the charging/discharging of the battery, respectively. We included the HVAC system and water-heater models because they

constitute a large part of the building energy consumption. The energy consumed by plug loads and lighting enter the simulation as uncontrollable disturbances.

This section provides a brief description of the simulation and reduced-order models used in the co-simulation, in addition to the objective function used by MPC to compute the optimal control inputs.

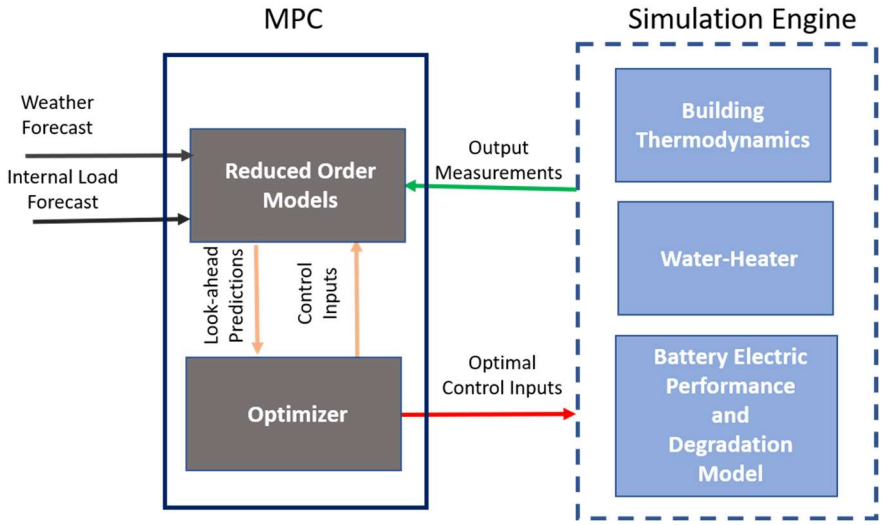

Figure 1. A flow diagram depicting the various components of the co-simulation environment.

Simulation Models

The co-simulation includes a building-envelope and heat-balance model in EnergyPlus, a two-node water-heater model, and a battery performance and degradation model. The components of the simulation engine serve as a substitute for the real building system. A description of the models is provided in the following sections.

EnergyPlus building model. The building-envelope model in EnergyPlus is of a large single-family home located in Fort Collins, Colorado. The home has a living space floor area of 166 m^2, an unfinished basement with floor area of 83 m^2, and a garage with a floor area of 44 m^2. The home is equipped with a single-speed air-source heat pump with a rated cooling capacity of 6.95 kW and a rated coefficient of performance (COP) of 5.4. During simulation, the heat pump is controlled with the help of a duty-cycle control input represented by U_{hvac} with a minimum on-time of 3 minutes. The simulation results are performed for the case where the battery is installed on an exterior wall. We assume the battery temperature to be equal to that of the outdoor ambient air. Although in actual practice the battery temperature would be different than that of the ambient air, this approximation provides a reasonable estimate of the impact of temperature on battery capacity

Water-heater model. We adopted a two-node water-heater model in this research from (Jin 2014). The model treats the water in the tank as consisting of two distinct layers with different temperatures, represented by T_1 and T_2 for the lower and upper levels, respectively. The two tank temperatures are modeled as a function of the water draw, V_d, supply water temperature, T_s, ambient temperature, T_{in}, and the energy consumed by the heating element, E_{wh}. The water-heater dynamics are represented using a discrete-time state-space matrix Equation (1)

$$x(k+1) = A_d x(k) + B_d u(k)$$
$$y(k) = C_d x(k) \quad (1)$$

where A_d, B_d, and C_d are the state-space matrices; k is the current timestep; $u = [E_{wh}, T_{in}, T_s]$ is the input vector; and x is the state vector representing the temperatures of the two water layers. The state space matrices, A_d and B_d, are time-varying functions of the water draw and are therefore computed at every simulation timestep. The water heater is controlled using a duty-cycle input represented by U_{wh}, and the heating energy provided by the element is shown in Equation (2).

$$E_{wh} = U_{wh} \cdot P_{wh,rated} \cdot t_s \quad (2)$$

where $P_{wh,rated}$ is the rater power of the heating element and $t_s$is the duration of the simulation timestep.

Battery electric performance and degradation model. The battery-performance model is used to describe the battery's aggregate properties, which include terminal voltage, state of charge, and temperature at every timestep of the simulation (1 minute). The literature on battery modeling consists of several different approaches of varying complexity ranging from high-fidelity models incorporating molecular-level physics to simple empirical-based models. The simulation system in this paper incorporates a model of a lithium-ion (Li-ion) battery with NMC chemistry (lithium nickel manganese cobalt oxide) developed in the System Advisor Model (SAM) (DiOrio 2015). The performance model in SAM is based on the work of Shepard (Shephard 1965) and Tremblay (Tremblay 2007) and intended to achieve a good balance between model complexity and computational feasibility. A brief description of the performance model is provided as follows.

The performance model simulates the battery terminal voltage to compute the battery charging or discharging power at each timestep. The terminal voltage, V_{term}, is expressed in Equation 3. A description of the variables in Equation 3 and the values of constants corresponding to a Li-ion cell in are shown in Tables 1 and 2, respectively. The values of the parameters are obtained from the model developed by Tremblay, (2007).

$$V_{term} = V_o - IR_{int} - K\left(\frac{Q_{max}}{Q_{max} - \int Idt}\right) + ae^{-B\int Idt} \quad (3)$$

We then compute the battery charging or discharging power in kilowatts, P_{bat}, in terms of the terminal voltage and battery current using the following equation:

$$P_{bat} = \frac{1}{1000} \cdot \eta_{bat} V_{term} I_{bat} \quad (4)$$

where η_{bat} is the charging or discharging efficiency and I_{bat} is the battery current used to charge or discharge the battery. At each timestep, k, the performance model also computes the SOC of the battery, Q_{bat}, as shown in Equation (5)

$$Q_{bat}(k) = Q_{bat}(k-1) + \left(\frac{1}{Q_{max}(k-1)}\right) \cdot P_{bat}(k-1) \quad (5)$$

where Q_{max} is the maximum capacity of the battery in kWh.

Table 1. Description of the variables in Equation (3).

Parameter (unit)	Description
V_{term}(V)	Terminal voltage
Q_{max}(Ah)	Battery capacity
I_{bat}(A)	Battery current
dt(hr)	Time-step

Table 2. Parameters of the terminal voltage equation.

Parameter	Description	Value
V_o	Open Circuit Voltage	3.7348
$R(\omega)$	Internal Resistance	0.09
$K(V)$	Polarization voltage	0.00876
$a(V)$	Exponential zone amplitude	0.468
$B(Ah)^{-1}$	Exponential zone time constant	3.5294

The total charge capacity of a battery degrades over time due to calendar aging and this degradation is accelerated by the charge and discharge cycles during operation. The lifetime model is used to predict this degradation under different operating conditions. This paper adopts the degradation model developed by (Smith 2017). The authors developed the model by measuring the degradation of Li-ion batteries under different operating conditions in a laboratory setting. One of the main advantages of incorporating this model is that it considers the effects of battery temperature. Adopting the model that incorporates temperature effects from Smith et al. (Smith 2017) is a key component of this research, as it enables development of optimal control strategies under different weather conditions and climatic locations.

We model the charge capacity degradation by taking into consideration two mechanisms: (1) the loss of cyclable lithium caused by formation of solid electrolyte interface (SEI), represented by Q_{max}^{li}, and (2) the mechanical damage of the negative electrode resulting from the charge/discharge cycles, Q_{max}^{neg}. The battery-capacity degradation due to each of the mechanisms is briefly described in the next section. The maximum available capacity in kilowatt-hours, represented by Q_{max}^{li} or Q_{max}^{neg}, factors in the instantaneous change in capacity due to ambient weather and the degradation over time.

The primary factor driving the formation of SEI is the calendar time, t, but formation is accelerated by factors such as state of charge at which the battery is stored, the depth of discharge during cycling, and the number of charge and discharge cycles. The battery charge capacity degradation due to the formation of SEI is shown in the Equation (6):

$$Q_{max}^{li} = d_o[b_0 - b_1 t^{\frac{1}{2}} - b_2 N - b_3\left(1 - \exp\left(-\frac{t}{\tau_{b_3}}\right)\right)] \quad (6)$$

where t is the calendar time in days, N is the total number of charge/discharge cycles over the battery's lifetime, and τ_{b_3} is an experimentally determined constant. Battery temperature affects the available maximum capacity at the current time instant as well as the rate of charge degradation.

Battery temperature affects the available maximum capacity at the current time instant as well as the rate of charge degradation. The parameter d_o captures the effect of the former, as shown in Equation (7). The variable T_{bat} represents the battery temperature, and $d0_{ref}, E_{a,d0,1}, R_{ug}, T_{ref}$, and $E_{a,do,2}$ were experimentally determined constants for a lithium-ion cell by Smith et al. (Smith 2017).

$$d_0 = d_{o,ref} \cdot \exp\left[-\frac{E_{a,do,1}}{R_{ug}}\left(\frac{1}{T_{bat}} - \frac{1}{T_{ref}}\right) - \left(\frac{E_{a,do,2}}{R_{ug}}\right)^2\left(\frac{1}{T_{bat}} - \frac{1}{T_{ref}}\right)^2\right] \quad (7)$$

The other parameters b_1, b_2, and b_3 model the capacity degradation and are functions of battery temperature, state of charge, open-circuit voltage, negative-electrode voltage, and maximum depth of discharge. The equation used to compute the parameter b_1 is shown as an example in Equation (8).

$$b_1 = b_{1,ref} \cdot \exp\left(-\frac{E_{a,b1}}{R_{ug}}\left(\frac{1}{T_{bat}} - \frac{1}{T_{ref}}\right)\right) \cdot \exp\left(-\frac{\alpha_{a,b1}F}{R_{ug}}\left(\frac{U_{neg}}{T_{bat}} - \frac{U_{ref}}{T_{ref}}\right)\right) \cdot \exp\left(\gamma \cdot (DOD_{max})^{\beta_{b1}}\right) \quad (8)$$

A detailed description of the other parameters and constants can be found in (Smith 2017). Figure 2 shows simulations of capacity degradation under different ambient conditions, at a battery charge/discharge cycle rate of 6 per day (Smith 2017).

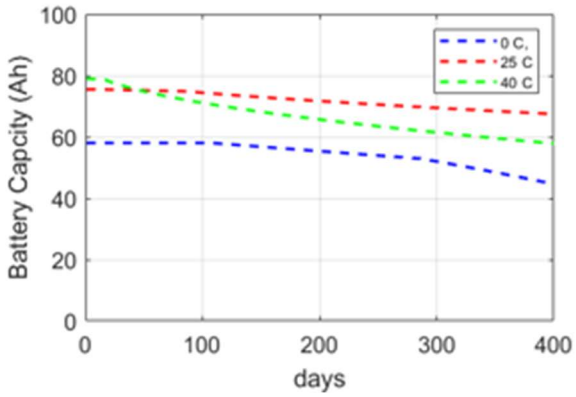

Figure 2. Capacity degradation under different operating conditions at a charge/discharge cycle rate of 6 per day.

Reduced-Order Models for MPC

The previous section provided a description of the models used to run the simulations. These models describe the dynamics of the each of the components (building thermodynamics, HVAC system, water-heater model, and battery) with a high degree of accuracy and serve as a substitute for the real-world system and a platform on which different control strategies can be tested. The

models, however, are highly nonlinear and nonconvex. In order to compute the optimal dispatch strategies in real time, we developed reduced-order models of the previously described components. The reduced-order models make the MPC objective function convex described ahead, and thus the problem of determining optimal dispatch strategies, more computationally feasible.

Room temperature model. The ARX model structure has been selected for the linear parametric approach to describe building thermodynamics as shown in Equation 10

$$y(k) = a_1 y(k-1) + a_2 y(k-2) + \cdots + b_1 u(k-1) + \cdots + b_{nb} u(k-n_b) + e(k) \quad (9)$$

where $y(k)$ is the output at timestep, k, u is the input, and e is random Gaussian noise used to capture the stochastic component of the model. The inputs and outputs of the ARX model described previously are shown in Equation 10

$$y = T_{in}; u = [T_{oa} - T_{in}, Q_{hvac}, Q_{internal}, Q_{solar}] \quad (10)$$

where T_{in} is the indoor air room temperature, T_{oa} is the outside air temperature, and Q_{hvac}, $Q_{internal}, Q_{solar}$ are the energy delivered by the HVAC system, internal heat loads, and window solar heat gain, respectively.

The parameters of the ARX model are obtained by training the model on historical simulation data spanning one month of the inputs and outputs of the building under consideration and performing regression analysis. The objective function used to perform regression analysis is defined as the sum of squares of the error between "measured" (in this case EnergyPlus-simulated) and predicted outputs, $T_{in}(k)$, as shown in Equation (11).

$$J_{arx} = \left(\frac{1}{N}\right) \sum_{i=1}^{N} \left(T_{in}(i) - \hat{T}_{in}(i)\right)^2 \quad (11)$$

where t is the current simulation timestep and n_p is the look-ahead horizon.

Linearized battery-degradation model. We used a Taylor series expansion to linearize the degradation of the battery as a function of the charging and discharging power of the battery.

Battery Control Algorithms

This section provides a description of the proposed MPC strategy together with a rule-based controller. We ran simulations using the rule-based controller as a baseline to quantify the improvement in terms of cost reduction and battery-life extension that can be achieved using the proposed MPC method.

Model Predictive Control. The first step in designing the MPC controller is to develop an objective function that outputs a single value that serves as a measure of the performance of the control system over a look-ahead horizon, referred to as a "control horizon." The performance variables considered in this research are the utility costs, occupant comfort, and battery degradation. The objective function is expressed as shown in Equation (12)

$$J_{mpc} = \sum_{i=k+1}^{N} r_{cost} \cdot \left(f_{util}(i) + f_{bat}(i)\right) + r_{comf} \cdot f_{comf}(i) \quad (12)$$

where k is the current simulation timestep; N is the number of timesteps in the control horizon; and f_{util}, f_{bat}, and f_{comf} are functions that measure utility cost, battery degradation cost, and occupancy discomfort, respectively. The utility cost function is simply the cost of the grid

electricity. The utility rate structure described in Table 4 is used to find the utility rate at the current timestep, $r_{util}(k)$, and is multiplied by the grid power, $P_{grid}(k)$, to obtain the utility cost as shown in Equation (13).

$$f_{util}(k) = r_{util}(k) \cdot P_{grid}(k) \quad (13)$$

The battery life span is assumed to be the time it takes for the capacity to degrade by 30%. The degradation cost of the battery from timestep i to $i+1$ is computed by multiplying the fraction of the usable capacity degraded in that period by the total cost of the battery: as shown in Equation (14).

$$f_{bat}(i) = \frac{1}{0.3} \cdot r_{bat} \Delta Q_{deg}(i+1|i) \quad (14)$$

The parameter r_{cost} of the MPC objective function in Equation 12 is assigned the value 0.18; the parameter r_{comf} is assigned a value 0.58 if the room temperature is too hot and 0.32 if too cold. The values of the parameters ensure that there are only a few instances where the room temperature lies outside the comfort band between 23.2°C (~74°F) and 25.6°C (~78°F). The parameters are subjective and can be tuned based on individual preferences. Lowering the value of r_{comf} results in greater instances of the room temperature being outside the comfort constraints but would also lower utility costs. We obtained these values based off the work done by Jin et al. (Jin 2017).

Rule-Based Control. A controller developed using a rule-based strategy serves as a baseline to compare the performance of the proposed MPC approach. A deadband control logic is used to operate the HVAC system. During cooling, the HVAC system is turned on whenever the room temperature, T_{in}, meets or exceeds the higher-threshold temperature, $T_{set-high}$, and turned off when the temperature reaches the lower threshold, T_{set-l} . The rules governing the rule-based controller for charging and discharging the battery are as follows:

- The charging and discharging power is never done simultaneously
- The battery is charged only from PV and never from the grid
- PV power is used to charge the battery only when this power is greater than the building load
- Grid power is used to furnish the additional power requirement when PV power is less than the building load
- The battery is discharged only during peak utility rate hours
- The battery discharge power is such that the usable charge is completely utilized during the peak hours.

In addition to these rules, certain additional constraints are imposed while charging and discharging the battery to ensure that the SOC is never outside the allowable minimum and maximum and the battery charging and discharging power are always less than the rated values.

Simulation Results and Discussion

The co-simulation platform was used to run several different test cases for the large single-family home, described earlier, with a grid-connected 4-kW PV system and a 3-kWh capacity/3-kW power battery storage system. The test cases are used to study the impact of

weather conditions, geographic location, and utility rate structure on battery degradation and utility costs. The building described earlier was used for running simulations corresponding to Fort Collins, Colorado. For other geographical locations, the layout of the building was kept constant, but certain efficiency measures such as wall insulation and heating and cooling efficiency were changed based on the DOE Zero Energy Ready Homes specifications, whose values were obtained from Jin (Jin 2020). Table 3 shows descriptions of some of the efficiency characteristics. Table 4 summarizes the climate zones of the locations studied and the TOU rate structures adopted in simulations corresponding to these locations. Detailed results of the first test case (i.e., summer weather conditions) with a TOU utility-rate structure are provided, followed by a summary of all the other simulation studies.

Table 3. Efficiency measures of the EnergyPlus models corresponding to the different geographic locations

Location	Fort Collins	Phoenix	Portland
Wall insulation	R-23	R-13	R-20
Unfinished attic	R-49	R-38	R-49
Windows	U = 0.3 SHGC = 0.3	U = 0.4 SHGC = 0.25	U = 0.3 SHGC = 0.46
Air leakage	3 ACH50	3 ACH50	2.5 ACH50

Table 4. Summary of climate zones and TOU rate structures for the three geographical locations investigated in this paper

Climate zone	Location	Summer rate structure	Winter rate structure
Cold	Fort Collins, CO	On peak: 2 p.m. to 7 p.m. Rate: $0.26/kWh Off peak: 7 p.m. to 2 p.m. Rate: $0.07/kWh	On peak: 5 p.m. to 9 p.m. Rate: $0.22/kWh Off peak: 9 p.m. to 5 p.m. Rate: $0.07/kWh
Hot-dry	Phoenix, AZ	On peak: 3 p.m. to 8 p.m. Rate: $0.243/kWh Rate: $0.109/kWh	On peak: 3 p.m. to 8 p.m. Rate: $0.231/kWh Off peak: 8 p.m. to 3 p.m. Rate: $0.109/kWh
Marine	Portland, OR	On peak: 3 p.m. to 8 p.m. Rate: $0.124/kWh Off peak: 8 p.m. to 3 p.m. Rate: $0.0413/kWh	On peak: 6 a.m. to 10 a.m. 5 p.m. to 8 p.m. Rate: $0.26/kWh Off peak: 10 p.m. to 6 a.m. 10 a.m. to 5 p.m. Rate: $0.07/kWh

Comparison of control strategies during summer in Fort Collins

The MPC objective function described earlier ensures that there are only a few occasions where the comfort constraints are violated (i.e., the room air temperature is above or below the desired set points). For example, Figure 3 shows the indoor air room temperature on a particular day in July in Fort Collins, when the maximum outside air temperature was 34°C (93.2°F), under the two MPC control strategies and the rule-based strategy. The MPC controller maintains the room temperature close to the upper temperature bound to minimize HVAC energy consumption. Modeling error and the difference in the simulation (1 minute) and control timesteps (15 minutes) cause the temperature to oscillate about this upper bound. In addition to maintaining the room temperature close to the upper bound, MPC minimizes utility costs by adopting precooling strategies. For example, Figure 3 also shows that the MPC controller starts cooling the room at around 1:30 p.m. to a temperature below the lower bound in order to reduce energy consumption and thereby the on-peak electricity prices, which start at 2 p.m.

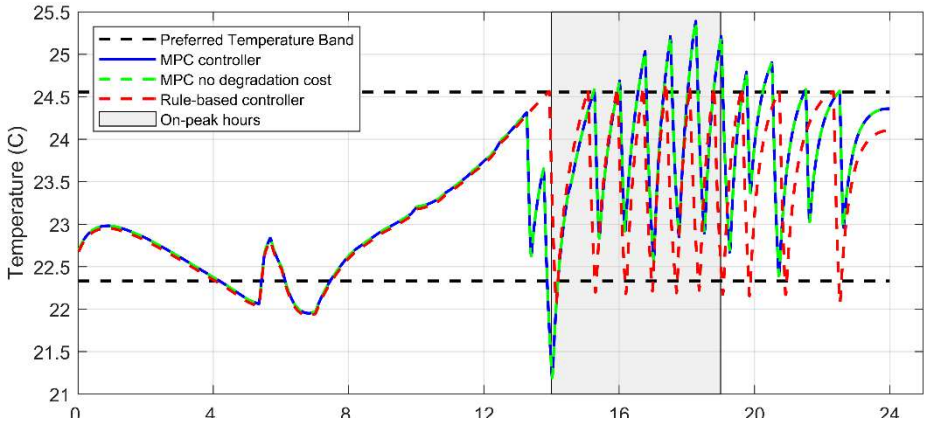

Figure 3. Comparison of room temperatures on July 5 using the three different controllers.

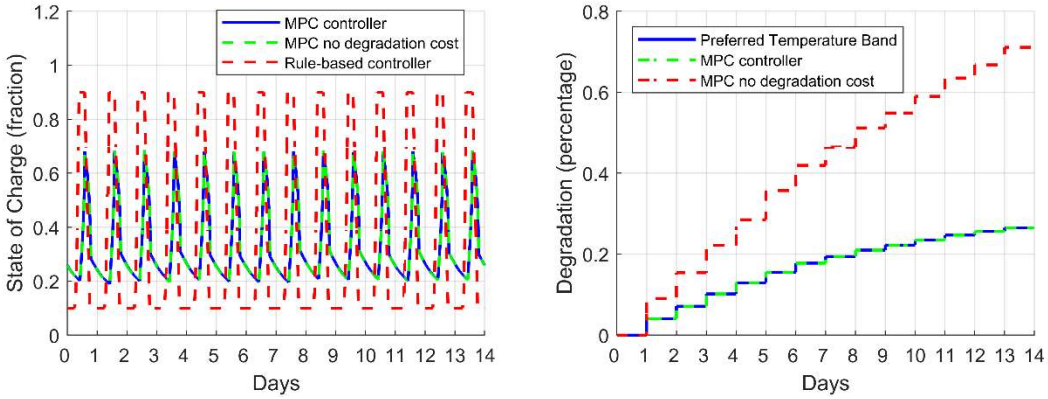

Figure 4. Battery state of charge and capacity degradation comparison from July 1–14 using the baseline controller and the two MPC controllers

Figure 4 shows the charging and discharging strategy adopted by the two MPC controllers and the baseline controller. The rate of battery degradation is significantly impacted by the DOD of each cycle. The number of cycles in both the baseline control strategy and the MPC strategies are equal, but due to much higher DOD, the rate of capacity degradation is approximately three times greater for the former. We also see that there is not much difference in the dispatch strategies of the two MPC controllers. MPC-I (objective function with degradation cost) would tend to lower the DOD for each battery charge and discharge cycle as compared to MPC-II (objective function with no degradation cost). However, the reduction in this particular case is imperceptible, as the benefits accrued by utilizing the stored battery energy during the peak hours outweigh the battery degradation costs.

Comparison of control strategies during winter in Fort Collins

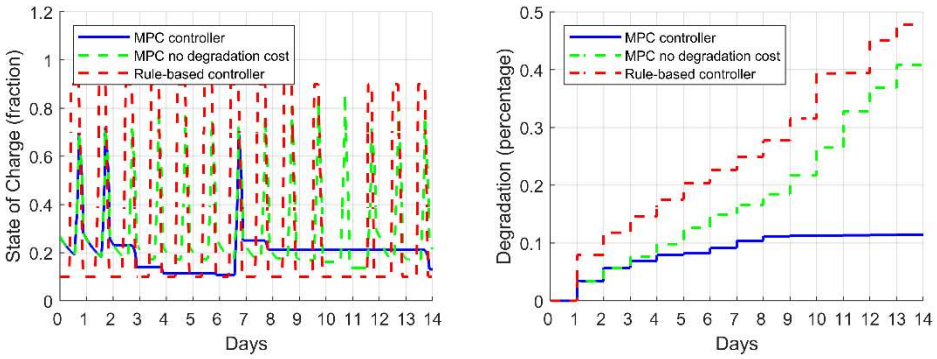

Figure 5. Battery state of charge and capacity degradation comparison from January1–14 using the baseline controller and the two MPC controllers

Referring back to Figure 2, we see that exposing the battery to cold temperatures (<0°C) not only reduces the available maximum capacity but also accelerates the rate of capacity degradation. The previous section showed that during the summer months, MPC-I and MPC-II compute similar dispatch strategies for the battery. During the winter months in Fort Collins, however, there is a significant difference in the dispatch strategies adopted by the two MPC controllers. Figure 5 shows a comparison on the battery state of charge and capacity degradation from January 1–14 using the three different control strategies. Due to the increased cost associated with capacity degradation in winter in Fort Collins, MPC-I utilizes the battery far less compared to MPC-II.

Comparison of control strategies at different geographical locations and weather conditions

We also ran simulations for Phoenix and Portland spanning 15 days during the months of January and July to compare the control strategies during winter and summer, respectively. Figure 6 shows the average capacity degradation per day, corresponding to the TOU rate structure described in Table 4 for summer and winter for the three locations studied. Owing to the greater rate of capacity degradation in cold-weather conditions, the battery usage with MPC-I is significantly lower during the winter months in Fort Collins and Portland. For Phoenix, which is in a hot-dry climate zone, the difference between the dispatch strategies of MPC-I and MPC-II vary imperceptibly, even during the winter months. A summary of the battery degradation costs per day is shown in Table 5 and a graphical representation of the combined average cost of battery degradation and utility prices per day is shown in Figure 7.

Table 5. Summary of battery degradation and utility costs

Location	Weather	Average battery degradation cost ($/day)		
		Baseline	MPC-I	MPC-II
Fort Collins	Summer	2.78	1.10	1.10
	Winter	1.67	0.40	1.41
Phoenix	Summer	3.58	2.09	2.09
	Winter	1.41	0.79	0.79
Portland	Summer	1.50	0.86	0.86
	Winter	2.01	0.28	0.93

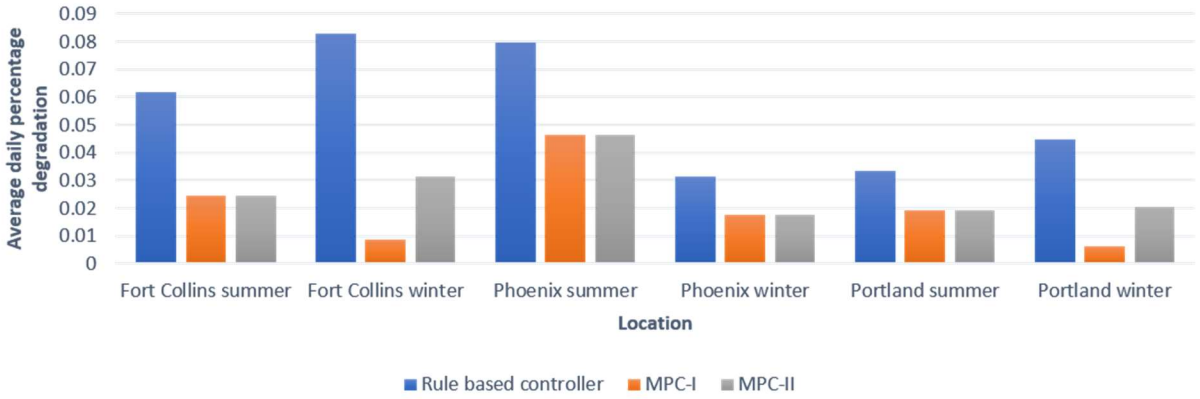

Figure 6. Comparison of the average battery capacity degradation per day at different geographical locations under different weather conditions

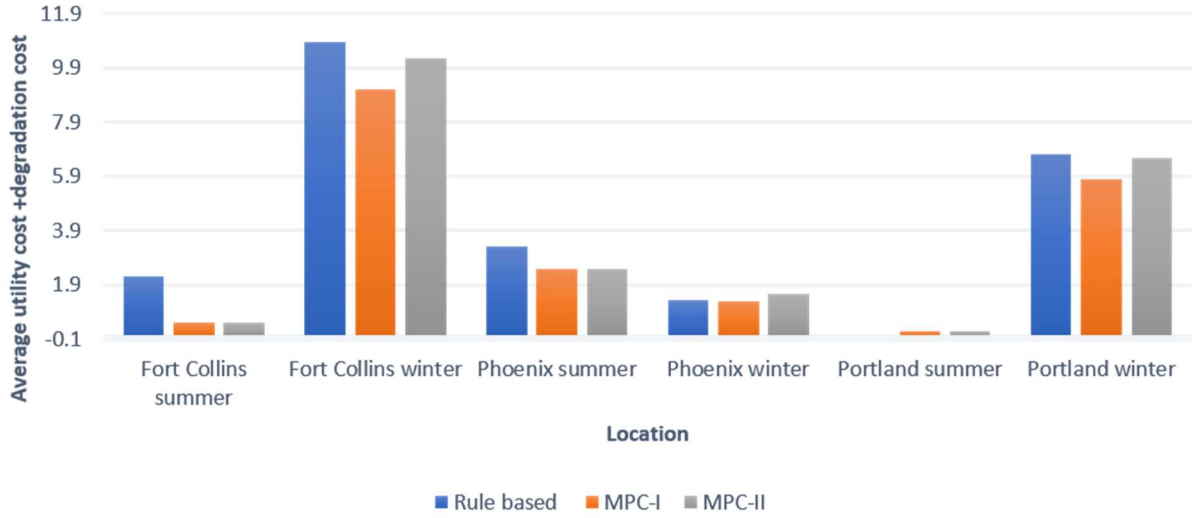

Figure 7. Comparison of the average battery capacity degradation per day at different geographical locations under different weather conditions

Conclusions

We developed a co-simulation platform by leveraging prior work done by Jin et al. (Jin 2017) and adding electric-performance and lifetime-degradation models of a lithium-ion battery with NMC chemistry. The battery models account for the effect of ambient temperature on capacity degradation, thereby enabling a study of dispatch strategies for building flexible loads and batteries under different weather and climatic conditions. We also added a linearized capacity degradation model using a Taylor series expansion to the co-simulation platform to enable MPC to compute optimal dispatch strategies over a look-ahead horizon using convex optimization.

We developed optimized dispatch strategies for a grid-connected PV home with a goal of extending battery life while simultaneously taking into consideration utility costs and occupancy comfort. We computed the optimized dispatch strategies for different operating conditions brought about by changing weather conditions, geographical locations, and utility pricing. We also used the co-simulation platform to compare the optimized strategies with the conventional strategies in terms of their impact on the utility costs and battery life span. The simulation results for this study show that the ambient conditions to which the battery is exposed has a significant impact on the capacity degradation. For the particular building under consideration, and the utility rate structure adopted in the simulations, simulation results suggest that battery dispatch strategies should take into consideration the capacity degradation, especially during cold-weather conditions.

References

Cai, J., H. Zhang, and X. Jin. 2019. "Aging-aware predictive control of pv-battery assets in buildings." *Applied Energy* 236: 478–488.

Comello, S., and S. Reichelstein. 2019. "The emergence of cost-effective battery storage." *Nature Communications* 10 (1): 1–9.

DiOrio, N., A. Dobos, S. Janzou, A. Nelson, and B. Lundstrom. 2015. *Technoeconomic modeling of battery energy storage in SAM*. Golden, CO: National Renewable Energy Laboratory. NREL/TP-6A20-64641.

Feldman, D. J., and R. M. Margolis. 2019. *Q4 2018/Q1 2019 Solar Industry Update*. Golden, CO: National Renewable Energy Lab. NREL/PR-6A20-73992.

Fitzgerald, G., J. Mandel, J. Morris, and H. Touati. 2015. *The economics of battery energy storage: How multi-use, customer-sited batteries deliver the most services and value to customers and the grid*. Basalt, CO: Rocky Mountain Institute.

Hoff, T., R. Perez, and R. Margolis. 2004. *Increasing the Value of Customer-Owned PV Systems Using Batteries*. Golden, CO: National Renewable Energy Laboratory. Internal Report.

Jin, X., J. Maguire, and D. Christensen. 2014. "Model predictive control of heat pump water heaters for energy efficiency." In *18th ACEEE Summer Study on Energy Efficiency in Buildings*: 133–145. Golden, CO: National Renewable Energy Laboratory.

Jin, X., K. Baker, D. Christensen, and S. Isley. 2011. "Foresee: A user-centric home energy management system for energy efficiency and demand response." *Applied Energy* 205: 1583–1595.

Li, J., and M. A. Danzer. 2014. "Optimal charge control strategies for stationary photovoltaic battery systems." *Journal of Power Sources* 258: 365–373.

Mishra, P.P., A. Latif, M. Emmanuel, Y. Shi, K. McKenna, K. Smith, and A. Nagarajan. 2020. "Analysis of degradation in residential battery energy storage systems for rate-based use-cases." *Applied Energy* 264: 114632.

Neukomm, M., V. Nubbe, and R. Fares. 2019. *Grid-Interactive Efficient Buildings*. Washington, D.C.: U.S. Department of Energy. DOE/EE-1968.

Nottrott, A., J. Kleissl, and B. Washom. 2013. "Energy dispatch schedule optimization and cost benefit analysis for grid-connected, photovoltaic-battery storage systems." *Renewable Energy* 55: 230–240.

Pascual, J., J. Barricarte, P. Sanchis, and L. Marroyo. 2015. "Energy management strategy for a renewable-based residential microgrid with generation and demand forecasting." *Applied Energy* 158: 12–25.

Riffonneau, Y., S. Bacha, F. Barruel, and S. Ploix. 2011. "Optimal power flow management for grid connected pv systems with batteries." *IEEE Transactions on Sustainable Energy* 2 (3): 309–320.

Shepherd, C. M. 1965. "Design of Primary and Secondary Cells. II. An Equation Describing Battery Discharge." *Journal of the Electrochemical Society* 112 (7): 657.

Smith, K., A. Saxon, M. Keyser, B. Lundstrom, Z. Cao, and A. Roc. 2017. "Life prediction model for grid-connected li-ion battery energy storage system." In *2017 American Control Conference (ACC)*: 4062–4028. Seattle, WA: IEEE.

Toledo, O. M., D. Oliveira Filho, and A. S. A. C. Diniz. 2010. "Distributed photovoltaic generation and energy storage systems: A review." *Renewable and Sustainable Energy Reviews* 14 (1): 506–511.

Tremblay, O., L.-A. Dessaint, and A.-I. Dekkiche. 2007. "A generic battery model for the dynamic simulation of hybrid electric vehicles." In *2007 IEEE Vehicle Power and Propulsion Conference*: 284–289. Arlington, TX: IEEE.

U.S. EIA (Energy Information Administration). 2018. *U.S. Battery Storage Market Trends*. Washington, D.C.: U.S. EIA.